Jurnal Teknologi

Full Paper

NUMERICAL INVESTIGATIONS ON COMBINED EFFECT OF WELDING RESIDUAL STRESS AND AXIAL COMPRESSIVE LOAD ON BUCKLING CAPACITY OF THIN LOW CARBON STEEL PLATES

Sivasubramaniyan N. S.[a,b,c], Sumanlal M. S.[a,b,d], Joy Varghese V. M.[a,b*]

[a]Department of Mechanical Engineering, College of Engineering Trivandrum, Kerala, India
[b]APJ Abdul Kalam Technological University, Thiruvananthapuram, Kerala, India
[c]All India Council for Technical Education, New Delhi, India
[d]Kerala State Council for Science Technology and Environment, Kerala, India

Article history
Received
23 October 2022
Received in revised form
15 May 2023
Accepted
19 June 2023
Published Online
21 August 2023

*Corresponding author
joyvarghesevm@cet.ac.in

Graphical abstract

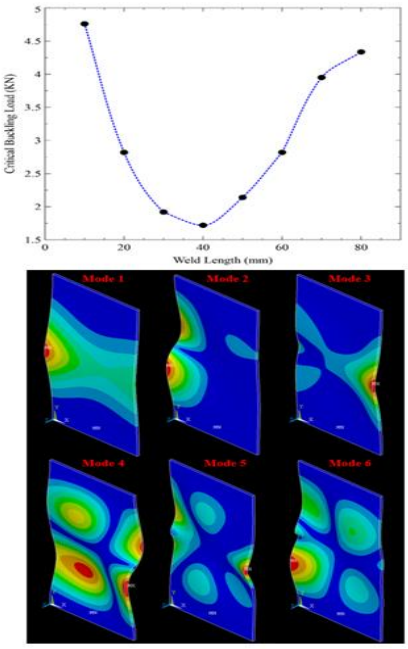

Abstract

Arc welding is the most commonly used metal joining process and its broad range of applications from large structural fabrications such as bridges to delicate satellite and aerospace components. Welding Residual Stress (WRS) and cracks developed during welding, reduce the quality of welds. Aerospace structures are normally fabricated using thin metal sheets to reduce mass and are always susceptible to buckling. Many researchers have published WRS numerical models and experimental validations, but the impact of WRS on the buckling of thin low carbon steel plates is yet to be studied. The main objective of this study is to analyse the influence of external compressive load and tendon force generated by welding residual stress on buckling strength of the TIG welded low-carbon steel plates. Linear buckling of welded plates under the combined effect of external compressive load and WRS generated due to various weld lengths were numerically modelled and its critical buckling loads are computed. The numerical simulation findings show that the critical buckling strength decreases by 80% when the weld length to plate width ratio (w/w_l) is equal to unity and it reduces to minimum when the w/w_l ratio is 0.5. After w/w_l ratio is 0.5, buckling strength increases and this behavior is caused by the stress field interaction that arises from both the applied axial compressive load and the WRS on the plate.

Keywords: Thermal Elastic-Plastic Analysis (TEP), Welding Residual Stress (WRS), welding distortion, eigen buckling, critical buckling load

1.0 INTRODUCTION

Thermo-mechanical modelling of Welding heat transfer and thereby forecasting the quality of weld is a subject that has garnered a lot of attention from both researchers and industrialists for the last few decades. The welding process imparts residual stress in welded components which may reduce the

structural integrity. The WRS and distortions cause problems not only in the final dimensional accuracy of welded structures but also decrease the structural integrity and significantly reduce the service life of materials. Therefore it is very important to consider the residual stresses while designing structures. Many researchers have published welding residual stress numerical models and experimental validations. Heat distribution models in which the welding heat source is assumed as a spatial distribution of heat and time can be used effectively to study the nature of induced WRS.

Rosenthal [1] proposed an analytical solution based on conduction heat transfer to predict the weld pool shape. Pavelic [1] introduced a 2D Gaussian type of heat distribution model with temperature-dependent properties, to analyse a two-dimensional plate, subject to GTA welding with surface radiation and convection. In 1984, Goldak *et al.* [1] proposed a 'double ellipsoid' configuration of the heat distribution model, which is capable of predicting shallow/deep penetration and even asymmetric welds. Gery D, *et al*. [2] studied the impact of welding speed and heat source characterstics on the thermal history of TIG welded low-carbon steel and concluded that fusion zone and Heat Affected Zone (HAZ) boundaries were sensitive to changes in heat source parameters. Various advancement in welding heat transfer numerical models and their limits was explained by Joy Varghese *et al.* [3].

Buckling is one of the most predominant modes of failure in thin slender structures such as beams, columns, pressure vessels, and aerospace structures. Several studies were carried out to arrive at closed-form solutions for the post-buckling of plates under different loading conditions. There are numerous studies carried out on the buckling of slender plates with imperfections such as holes, cracks, welds etc. which shows more influence on its buckling strength.

Moen *et al.* [4] developed closed-form expressions for critical buckling stress including the influence of multiple holes on the plates under bending or compression. Khedmati *et al.* [5] numerically studied the variation in buckling strength in a plate with crack subjected to an axial compressive load by varying crack length, position, plate aspect ratio and orientation, and the numerical simulation shows significant influence of each variable on the buckling strength of the cracked plate under compressive load. Jahanpour *et al*. [6], suggested a formula for a simply supported rectangular plate under biaxial and shear loads using energy method. Buckling load prediction was carried out using the regression and interpolation techniques and formulated a simple equation with minimum error for simply supported rectangular plate under biaxial and shear loads. M.H. Taheri *et al.* [7] carried out numerical and experimental studies on the buckling stability of aluminium alloy plates with off-centre cracks of different sizes, subjected to axial compressive load and concluded that the impact of eccentric crack largely depends on the support type used for constraining plate.

N. Chakravarthy *et al.* [8] conducted studies to enchance the load carrying capacity of cold formed steel member by providing CFRP reinforcement and showed an increase in load carrying capacity and a reduction in deflection due to CFRP strengthening. H. Fan *et al.* [9] applies a buckling design method based on the energy barrier approach to axially compressed stiffened cylindrical shells. H. Fan *et al.* investigates the effects of different structural parameters on imperfection sensitivity and design buckling loads, and successfully obtains stiffened cylindrical shells with high design buckling loads and low imperfection sensitivity, which are favorable for lightweight design.

Various studies were carried out to understand the influence of the welding process on buckling strength. Deo *et al.* [10] conducted numerical and experimental analysis, to predict welding-induced distortion of a fillet weld, followed by Eigenvalue finite element analyses to understand buckling distortion and observed that buckling distortion occurs if the critical buckling stress is lower than the residual stress for a given weld size. C. L. Tsai *et al.* [11] studied the buckling evolution process on AH36 steel using an integrated experimental and numerical approach and concluded that by using the maximum longitudinal inherent shrinkage strains, the critical buckling factor can be computed from eigenvalue finite element analysis. Wang *et al*. [12] studied the welding-induced buckling mechanism with the help of Eigenvalue analysis and inherent deformation theory-based elastic Finite Element (FE) analysis. In the work of Yang *et al.* [13], the local-overall interactive buckling behaviour of welded square and rectangle hollow sections was studied experimentally and validated developed FE model with experimental welding residual stress distribution data obtained from the literature.

Cao. *et al.* [14] conducted a finite element analysis to examine the effects of the width-to-thickness ratios of plates, slenderness, and steel grade on the local buckling load and ultimate load of HSS welded I-section stub columns under axial compression. The findings reveal that the width-to-thickness ratios of plates have a noteworthy impact on the stress ratios σ_{cr}/f_y and σ_u/f_y. Moreover, the stress ratio σ_{cr}/f_y decreases as the slenderness and steel grade increase. Rastgar *et al*. [15] did a field study on the effect of vertical weld imperfections in storage tanks under uniform external pressure and concluded that 65% of the buckling load obtained from the ASME Code should be used for steel tanks designed under uniform external pressure. H. Fang *et al.* [16] studied the effect of RS for various combinations of bending and compression and observed minimum effect of residual stresses over members with slenderness values between 0.7 and 1.1. Y. Chen *et al*. [17] studied the buckling behaviour of π-shaped welded columns under axial compression and shows a large deviation in numerical results from experimental results when the longitudinal residual stress was not considered. X. Wang *et al.* [18] studied the buckling of Aluminum extruded panels considering welding geometrical effects. J. Wang *et al.* [19]studied the influence of clamping over buckling distortion using WRS obtained from TEP analysis.

Most of the Studies related to buckling due to welding are conducted by using WRS values from

either experimental data for a few measured points or from closed-form solutions for WRS. This kind of approach only provides an approximate result for the buckling problem, since the WRS field is highly complex and non-linear in nature. Also, WRS depend on the size and type of restraint applied over the structure during welding. Some of the studies such as C. L. Tsai *et al.* [11] used a TEP model for simulating the welding process which gives a complex WRS field based on the welding parameter. In this study, the impact of WRS on the buckling strength of the low-carbon steel plates is carried out numerically. The TEP model is used for modelling residual stress developed during the TIG welding process and linear buckling analysis of welded plates undergoing various welding sequences and different weld lengths were modelled and its critical buckling strength are computed numerically.

2.0 METHODOLOGY

2.1 Thermal Elastic-Plastic (TEP) Analysis Material Properties

The study is conducted on low carbon steel and temperature-dependent properties reported by Chidiac *et al*. [20], T. L. Teng *et al.* [21] and Z. Barsoum *et al.* [22] are used for numerical simulation. Density of low carbon steel is assumed as 7850 Kg/m^3. The temperature-dependent thermal and mechanical properties used for modelling thermo structural simulation are shown in Table 1 and Table 2.

Table 1 Thermal properties of low carbon steel (EN3B steel)

Temperature (°C)	25	200	500	650	1000	1500	3000
Thermal Conductivity (Wm^{-1} K^{-1})	49	46	28	26	29	33	61
Enthalpy (x10^7 Jm^{-3})	11	55	243	336	497	856	1396
Specific Heat (J Kg^{-1}K^{-1})	455	524	1381	812	627	8678	830

Table 2 Mechanical properties of low carbon steel (EN3B steel)

Temperature (°C)	Young's Modulus (GPa)	Poisson's ratio	Yield Strength (MPa)	Tensile Strength (MPa)	Thermal Expansion Coefficient (× 10^{-6} K^{-1})
25	209	0.29	418	623	32
200	200	0.30	313	501	33
500	163	0.31	124	210	37
650	143	0.33	82	134	38
700	137	0.33	79	125	39
1000	106	0.35	-	-	42
1500	-	0.48	-	-	44

Heat Source Model

Goldak's Gaussian double ellipsoidal heat distribution model for moving welding heat source as in reported in Klobcar D, *et al.* [23] is used for the numerical simulation and shown in Eqn.1.

$$Q(x,y,z,t) = \frac{6\sqrt{3}f_i\eta UI}{abc\pi\sqrt{\pi}} e^{\left[-3\left(\frac{x-vt}{a_i}\right)^2-3\left(\frac{y}{b}\right)^2-3\left(\frac{z}{c}\right)^2\right]} \quad (1)$$

Where *U, I, v, t, f_i,*and η are welding voltage (V), welding current (A), welding speed (mm/s), time (s), fraction of heat deposited in weld region, and heat source efficiency respectively. a_i, b and c are the constant which defines the characteristics of the welding heat source and their values are selected concerning actual weld pool dimensions measured during welding (as per Wahab. M.A, *et al.* [24]). The parameters and constants for numerical simulation of Autogenous TIG welding process used for welding 2 mm thick plates are shown in Table 3.

Table 3 Heat source parameter and constants for numerical simulation

U (V)	I (A)	v (mm /s)	η	f_f	f_r	a_f (mm)	a_r (mm)	b (mm)	c (mm)
9	75	5	0.8	1.4	0.6	3	7	2.5	2

Numerical Model Validation

The validation of the FE model presented in this study is carried out by comparing it with the experimental data from Chen *et al.*'s work [25]. In their work, the X-ray diffraction technique was used to measure the WRS developed over a 4 mm thick steel plate. To validate the numerical model, the plate dimensions (300×250×4 mm), boundary conditions and heat source parameters used in Chen *et al.*'s work are adopted, where the plate is clamped at its four corners. The Figure 1 shows the validation of the current numerical model.

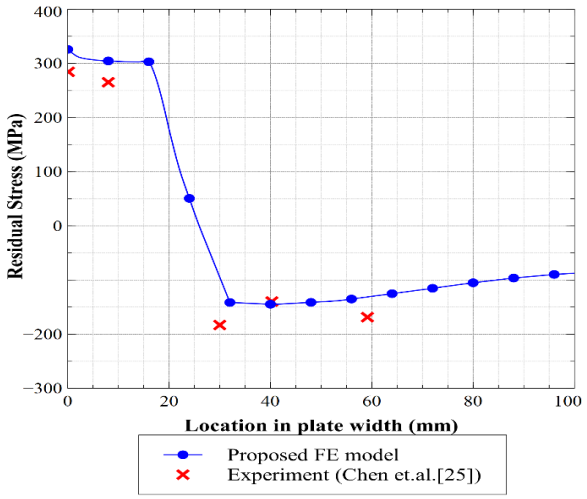

Figure 1 Numerical Model Validation

FE Model and Boundary Conditions

Uncoupled thermal and structural analysis is employed for obtaining WRS, in which thermal and structural analysis are carried out separately. The temperature distribution obtained from the thermal analysis is applied to the structural analysis as Nodal temperature load. Detailed flow chart of numerical simulation is shown in Figure 2.

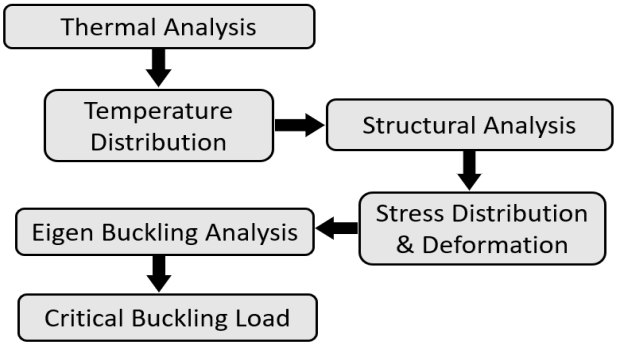

Figure 2 Methodology of Numerical Simulation

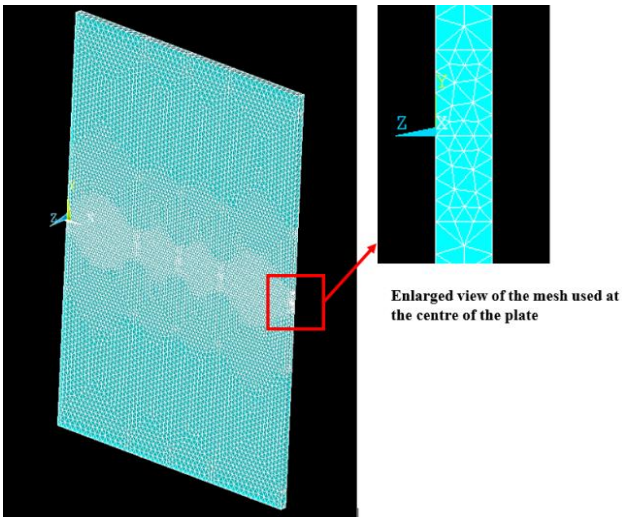

Figure 3 FE Mesh used in TEP Analysis

For this study, Mild steel plate 2 mm thick, 80 mm wide and 160 mm long are used. The entire simulation is carried out in ANSYS APDL using 20 noded Brick elements (Solid90 for thermal analysis and Solid186 for structural analysis). Same mesh is employed for thermal and structural analysis. For Augenous TIG welding, no filler rod is used and same material properties mention in Table 1 and Table 2 are assigned for the entire domain of the FE model.

The meshed FE model have 70702 nodes and 41377 elements and is shown in Figure 3, with a fine mesh at the middle of the plate along the weld line and considerably coarse mesh in areas away from the weld line. A horizontal weld is made along the centre of the plate and AA', BB', CC' and MM' are the path lines as shown in Figure 5, along which the results are extracted from the numerical model.

Heat distribution function shown in eqn. 1 is applied as heat generation on the top surface for TIG welding heat source and combined convective and radiative heat transfer equation as suggested by Chidiac *et al*. [20] are used as the boundary condition for thermal analysis. Room temperature is assumed as 25°C. For Structural analysis, all Degrees of Freedom (DOF) are arrested on the top and bottom surface of the plate symmetrically for entire weld length as shown in Figure 4 and temperature field computed from the thermal analysis is applied as thermal load for structural analysis.

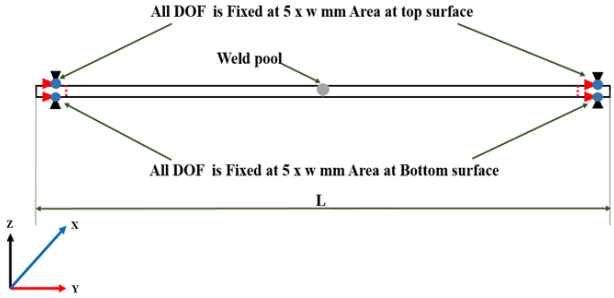

Figure 4 Boundary condition for structural analysis part of TEP analysis

2.2 Welding Cases

Studies are conducted to understand the influence of weld length on the buckling strength of the welded plates. In this study, Weld length (as shown in Figure 5) along the weld direction is varied from 80 mm (entire plate width, w_l) to 10 mm at the centre of the plate.

2.3 Static and Eigenvalue Buckling Analysis

Mesh used for Thermal Elastic-Plastic Analysis (TEP) is employed for both Static and Eigenvalue buckling analysis. After TEP analysis, static analysis is done on the model by applying an axial compressive load of 1 KN and then buckling analysis is carried out. Buckling analysis for each weld length case as in section 2.4 is carried out by considering WRS obtained from respective TEP analysis and 1 KN axial compressive

load. Constraints applied to the plate for undergoing Static and Eigenvalue buckling study are shown in Figure 5.

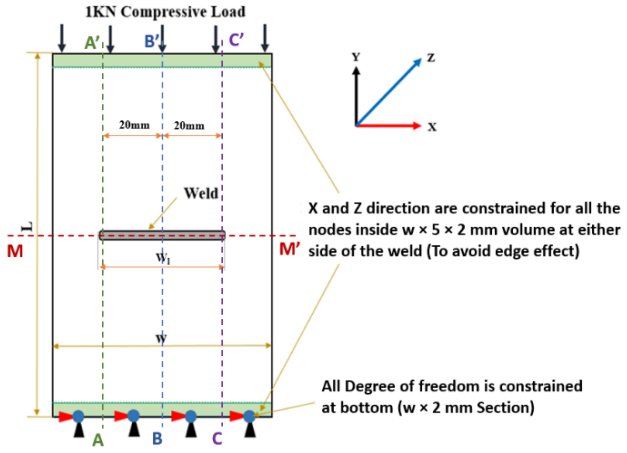

Figure 5 Boundary condition for Static & Eigen buckling analysis

3.0 RESULTS AND DISCUSSION

TEP Analysis and Eigenvalue Buckling analysis for various weld length cases (as discussed in section 2.2) are conducted and observations from the numerical study are mentioned in the current section.

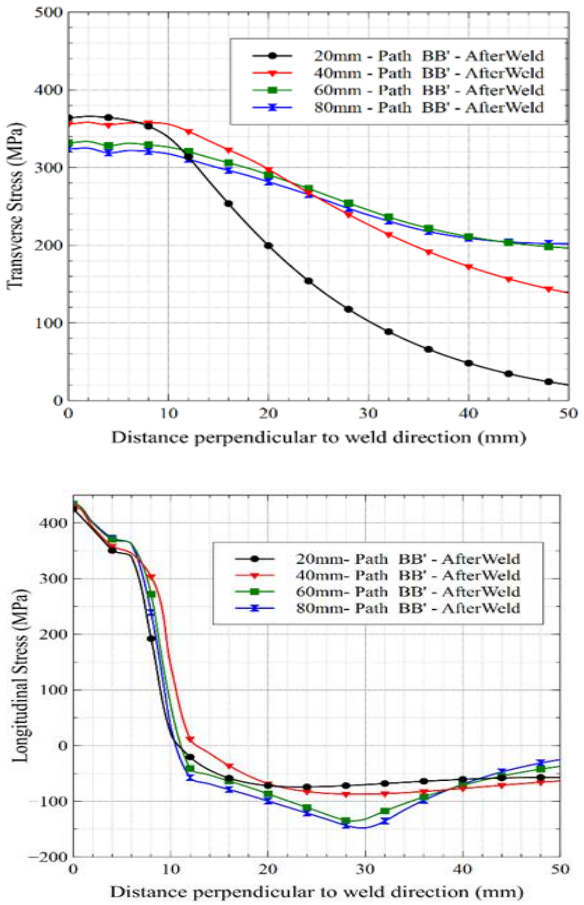

Figure 6 Variation of residual stress with weld length along path BB'

Longitudinal and transverse stress along path BB' (as shown in Figure 3) for 20 mm, 40 mm, 60 mm, and 80 mm weld lengths are shown in Figure 6. For all weld length cases, maximum longitudinal and transverse stress are observed at weld zone. Also, longitudinal stress becomes compressive after 10 mm (HAZ) from the weld centre. Longitudinal stress shows a similar trend in stress distribution along the plate, but transverse stress varies with weld length. As weld length decreases, the deviation of transverse stress along the plate increases. This is due to the presence of unwelded portions at either side of the weld along weld direction.

From Figure 7, distortion of the plate increases with an increase in weld length. Due to welding operation, the flat plate deforms to a convex shape. Also, it observed that the distortion progressively increases along weld direction for above 60 mm welds, but up to 50 mm weld distortion is more at BB' path.

From the static analysis result, variations in longitudinal and transverse residual stress distribution along path MM' over welded plate before and after the application of 1KN load are shown in Figure 8. Up to 20 mm weld length, both longitudinal and transverse stress has no significant variation on the application of load. But for increased weld length, a reduction in transverse stress is observed during the application of load. This is due to the portion of applied load shared between welded and unwelded portions of welded plates (Interaction of stress field). Up to 20 mm, the unwelded region takes most of the load applied. i.e., when weld length increases, the unwelded region reduces. So, more load should be taken across welded portion and hence there will be tensile stress reduction in the transverse direction.

Application of axial load modifies the WRS field that exists on the welded plate. Since axial load is applied along the transverse direction (y direction), a large variation in transverse stress field is observed and is shown in Figure 10. Contour plots of transverse stress field for 20 mm, 40 mm, 60 mm and 80 mm welded plates, explain the distribution of compressive load. Table 4. shows the variation of transverse stresses on the welded and unwelded portion of the welded plates before and after the load application. As the weld length increases, magnitude of tensile transverse stress decreases due to the applied load.

Eigenvalue buckling analyses are conducted on the welded plate with all weld length cases individually as mentioned in section 2.3. For the first buckling mode, critical buckling load of welded plates with varying weld length are shown in Figure 9. Table 5 depicts the critical buckling loads for the first six modes of buckling of both unwelded and welded (for each weld length) plates. Figure 11 shows the buckling shapes of a welded plate with full-width weld (80 mm).

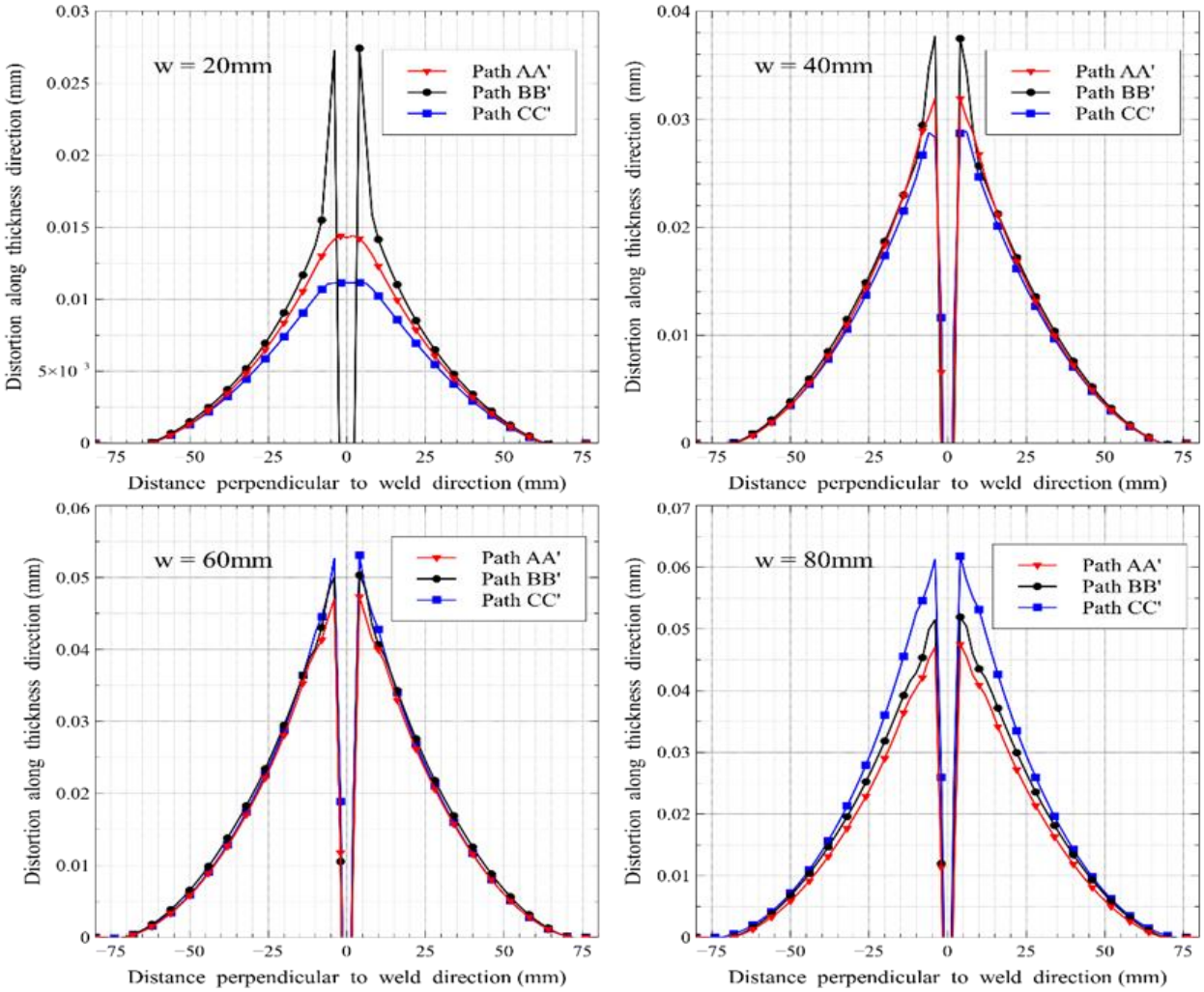

Figure 7 Distortion along thickness direction due to 20, 40, 60 and 80 mm weld length respectively

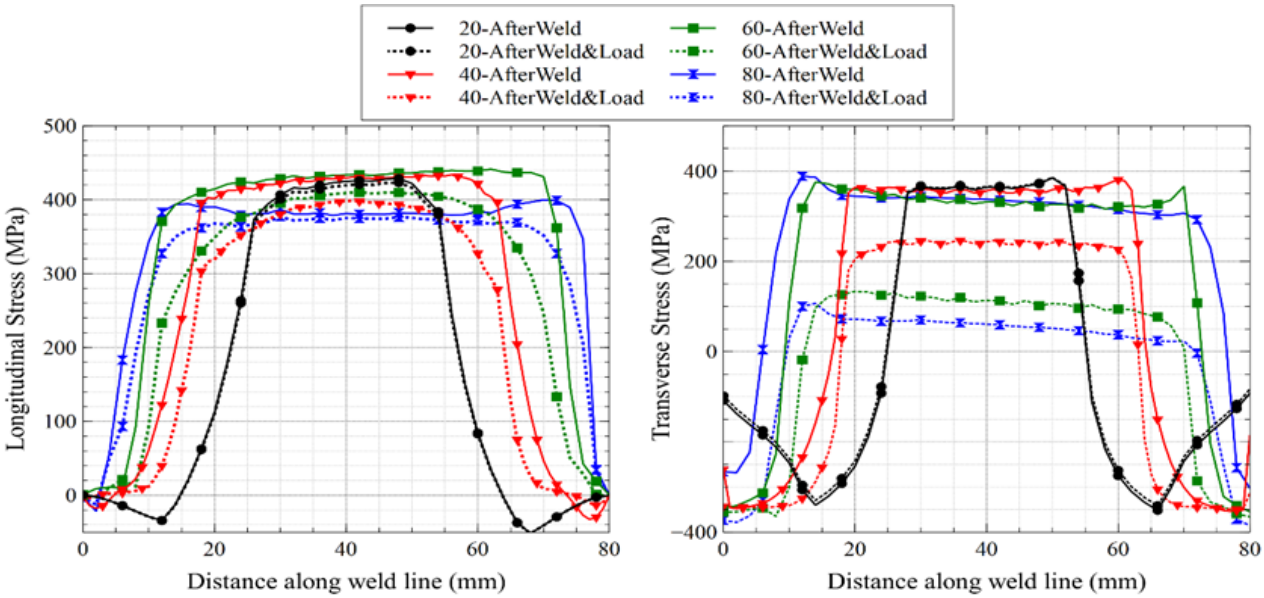

Figure 8 Residual stress distribution along weld direction (Path MM') for before and after static loading

Table 4 Variation in transverse stresses (in MPa) on the welded and unwelded portions of the plate

Region	Weld length = 20 mm		Weld length = 40 mm		Weld length = 60 mm		Weld length = 80 mm	
	Before Loading	After Loading	Before Loading	After Loading	Before Loading	After Loading	Before Loading	After Loading
Welded	394	392	399	266	388	147	416	133
Unwelded	59	62	147	59	222	138	255	15

Table 5 Variation of critical buckling load with weld length for first six mode

Mode	Critical Buckling Load (KN)								
	w = 0	w = 10 mm	w = 20 mm	w = 30 mm	w = 40 mm	w = 50 mm	w = 60 mm	w = 70 mm	w = 80 mm
1	20.60	4.76	2.82	1.92	1.72	2.14	2.82	3.95	4.34
2	42.25	7.47	4.15	2.7	2.36	3.13	4.17	5.92	6.55
3	53.84	7.68	4.26	2.99	2.74	3.24	4.75	6.97	8.22
4	75.35	8.85	4.84	3.32	2.98	3.82	5.8	8.45	10.28
5	83.11	16.19	8.85	5.72	4.99	6.1	7.9	10.24	11.88
6	116.47	20.59	10.98	7.09	5.78	6.81	8.55	10.46	12

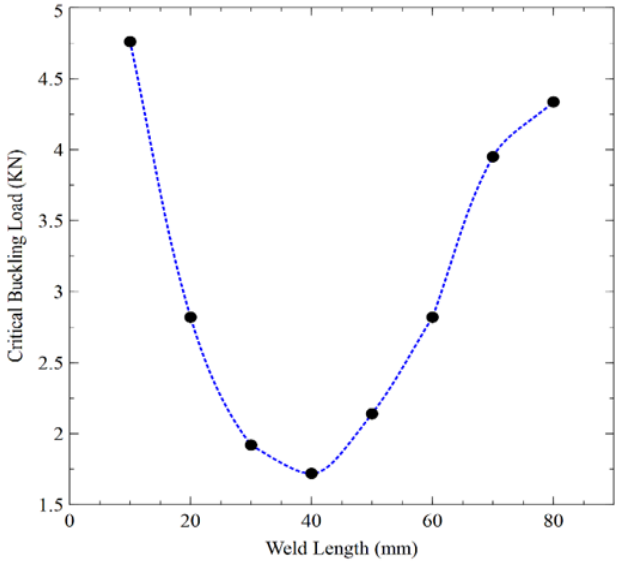

Figure 9 Critical buckling load for Mode 1 buckling of welded plates with varying weld length

From this study, the critical buckling load for an unwelded plate is observed as 20.60 KN and its values are reduced by nearly 79% when the full-width weld is introduced into the plate. The minimum critical buckling load observed for 40 mm weld length is 1.72 KN (90% reduction compared to that of the unwelded plate). When the weld length is increased from 10mm to 80 mm, initially up to 40 mm weld length, critical buckling load decreases gradually and after 40 mm, its value increases gradually. But the welding distortion in the plate increases with increase in weld length.

From the numerical results shown in Figure 8, figure 10 and table 4, a large portion of the load is distributed across the welded portion of the plate after 40 mm weld length. Up to 20 mm weld length, the majority of the load is distributed across the unwelded portion of the plate. For 30 mm and 40 mm weld length cases, there exist high-stress concentration regions at either side of the weld seam along weld direction due to interaction between developed stresses at unwelded and welded portions of same welded plates at either side weld seam. This formation of stress concentration region led to a drop in critical buckling load for 30 mm and 40 mm weld length cases.

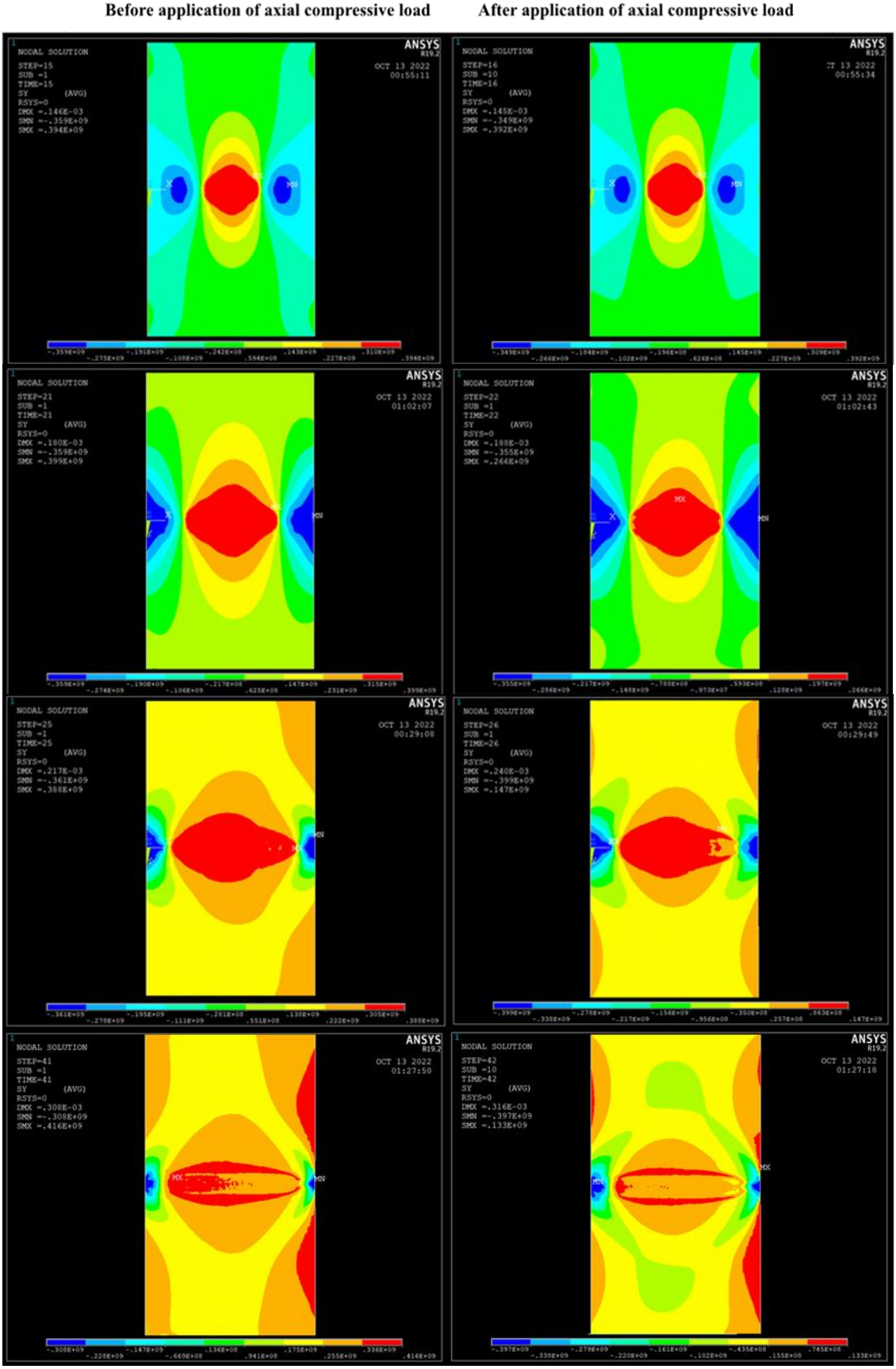

Figure 10 Transverse stress distribution before and after application of axial compressive load for weld lengths (a)20 mm (b)40 mm (c) 60 mm and (d) 80 mm

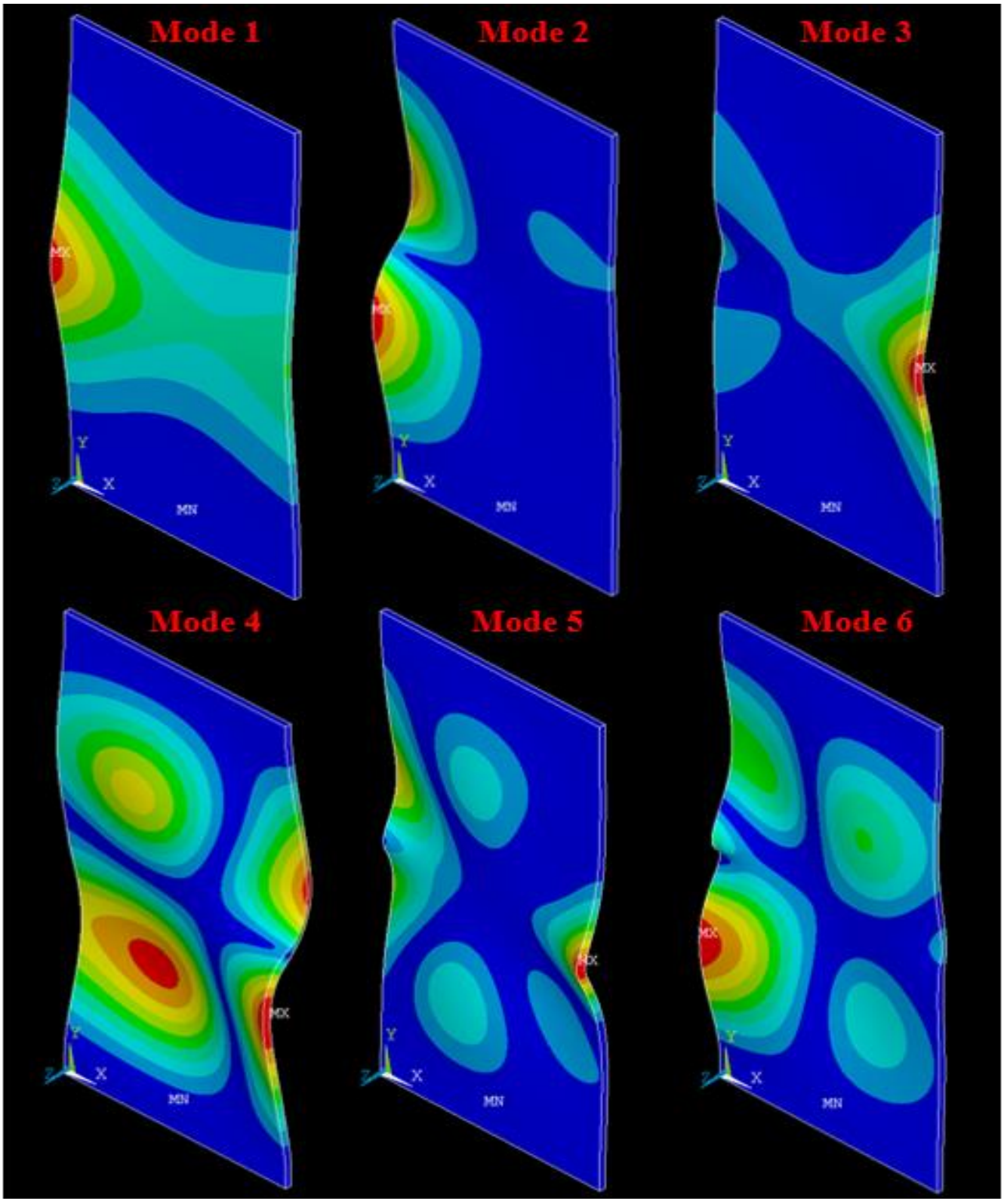

Figure 11 Buckling Mode Shapes for welded Plates with 80mm length weld

5.0 CONCLUSIONS

The influence of external compressive load and tendon force generated by welding residual stress on buckling strength of welded plate is studied numerically. From the numerical simulation results, the deviation of transverse stress along the plate away from weld region increases as weld length decreases.

This is due to the presence of unwelded portions at either side of the weld along weld direction which imparts large compressive stress region in the plate. The presence of this stress region has higher influence on transverse stress field. From static analysis, application of 1 KN load affects the trasverse WRS distribution significaticantly as the weld length increases. From Eigenvalue buckling analysis, An 80% reduction in critical buckling strength is observed, when weld length to plate width ratio (w/w_l) is unity. Minimum critical buckling load is observed when w/w_l ratio becomes 0.5. This phenomenon is caused by the influence of the interaction of stress field developed on the plate due to both welding and applied axial compressive load. Above 0.5 w/w_l ratio, the presence of tensile component (due to tendon force) of transverse WRS developed along the weld improves the buckling strength of thin welded plates with weld length significantly.

Based on this study, it can be inferred that the buckling strength of a welded component is greatly affected by both the WRS distribution and welding distortion. Therefore, it should be considered in the thermo structural simulation for welding process, while predicting the buckling strength of the thin welded structure. Also, conclude that conducting small repair welds have a signficant impact on the structural stability of thin welded structures with its weld length. The influence of filler material and weld length to thickness of plate is not considered in this study. In future, present FE model can be improved for conducting homogenous and heterogenous welding on different material with different plate thickness.

Conflicts of Interest

The author(s) declare(s) that there is no conflict of interest regarding the publication of this paper.

Acknowledgements

The author like to express his sincere gratitude towards the All India Council for Technical Education (AICTE), New Delhi, India, for providing PhD fellowship under AICTE Doctoral Fellowship (NDF/ADF) Scheme. The author would also like to sincerely acknowledge support from the Kerala State Council for Science Technology and Environment (KSCSTE), College of Engineering Trivandrum & APJ Abdul Kalam Technological University, Thiruvananthapuram, India for carrying out the research work.

References

[1] J. Goldak, A. Chakravarti, and M. Bibby. 1984. A New Finite Element Model for Welding Heat Sources. *Metallurgical Transactions B.* 15B: 299-305. Doi: 10.1007/BF02667333

[2] D. Gery, H. Long, and P. Maropoulos. 2005. Effects of Welding Speed, Energy Input and Heat Source Distribution on Temperature Variations in Butt Joint Welding. *J Mater Process Technol*. 167(2-3): 393-401. Doi: 10.1016/j.jmatprotec.2005.06.018.

[3] V. M. Joy Varghese, M. R. Suresh, and D. S. Kumar. 2013. Recent Developments in Modeling of Heat Transfer During TIG Welding - A Review. *International Journal of Advanced Manufacturing Technology*. 64(5-8): 749-754. Doi: 10.1007/s00170-012-4048-9.

[4] C. D. Moen and B. W. Schafer. 2009. Elastic Buckling of Thin Plates with Holes in Compression or Bending. *Thin-Walled Structures*. 47(12): 1597-1607. Doi: 10.1016/j.tws.2009.05.001.

[5] M. R. Khedmati, P. Edalat, and M. Javidruzi. 2009. Sensitivity Analysis of the Elastic Buckling of Cracked Plate Elements Under Axial Compression. *Thin-Walled Structures*. 47(5): 522-536. Doi: 10.1016/j.tws.2008.10.018.

[6] A. Jahanpour and F. Roozbahani, 'An applicable formula for elastic buckling of rectangular plates under biaxial and shear loads', Aerosp Sci Technol, vol. 56, pp. 100–111, Sep. 2016, DOI: 10.1016/j.ast.2016.07.005.

[7] M. H. Taheri and P. Memarzadeh. (2020). Experimental and Numerical Study of Compressive Buckling Stability of Plates with Off-center Crack. *Theoretical and Applied Fracture Mechanics*. 109: 102706. Doi: 10.1016/j.tafmec.2020.102706.

[8] N. Chakravarthy, S. Naganathan, J. Aun, S. Kalavagunta, K. N. Mustapha and T.R. Veena, 'Experimental investigation of CFRP strengthened I-shaped cold formed steel beams', Jurnal Teknologi, vol. 79(5), pp. 83-89, 2017, DOI: 10.11113/jt.v79.10255.

[9] H. Fan, L. Li, W. Gu, P. Liu, and D. Hu. 2022. Buckling Design of Stiffened Cylindrical Shells Under Axial Compression Based on Energy Barrier Approach. *Thin-Walled Structures.* 179: 109667. Doi: 10.1016/j.tws.2022.109667.

[10] M. V. Deo, P. Michaleris, and J. Sun. 2003. Prediction of Buckling Distortion of Welded Structures. *Science and Technology of Welding and Joining*. 8(1): 55-61. Doi: 10.1179/13621710322500900.

[11] C. L. Tsai and M. S. Han. 2004. Thermal and Mechanical Evolution of Welding-Induced Buckling Distortion. *Journal of the Chinese Institute of Engineers.* 27(6): 907-920. Doi: 10.1080/02533839.2004.9670943.

[12] J. Wang, S. Rashed, and H. Murakawa. 2014. Mechanism Investigation of Welding Induced Buckling Using Inherent Deformation Method. *Thin-Walled Structures.* 80: 103-119. Doi: 10.1016/j.tws.2014.03.003.

[13] L. Yang, G. Shi, M. Zhao, and W. Zhou. 2017. Research on Interactive Buckling Behavior of Welded Steel Box-section Columns. *Thin-Walled Structures*. 115: 34-47. Doi: 10.1016/j.tws.2017.01.030.

[14] X. Cao, S. Liu, C. Cheng, R. Zhong, Z. Tao, X. Zhou, and Z. Kong. 2022. Numerical Simulation for Local Buckling Behaviour of HSS Welded I-section Columns Under Axial Compression. *Thin-Walled Structures*. 174: 109060. Doi: 10.1016/j.tws.2022.109060.

[15] M. Rastgar and H. Showkati. 2018. Buckling Behavior of Cylindrical Steel Tanks with Concavity of Vertical Weld Line Imperfection. *J Constr Steel Res.* 145: 289-299. Doi: 10.1016/j.jcsr.2018.02.028.

[16] H. Fang and T. M. Chan. 2019. Buckling Resistance of Welded High-strength-steel Box-section Members Under Combined Compression and Bending. *J Constr Steel Res.* 162: 105711. Doi: 10.1016/j.jcsr.2019.105711.

[17] Y. Chen, G. Shu, B. Zheng, and R. Lu. 2020. Overall Buckling Behaviour of Welded π-shaped Compression Columns. *J Constr Steel Res*. 165: 105891. Doi: 10.1016/j.jcsr.2019.105891.

[18] X. Wang, J. Amdahl, and O. Egeland. 2022. Numerical Study on Buckling of Aluminum Extruded Panels Considering Welding Effects. *Marine Structures.* 84: 103230, Doi: 10.1016/j.marstruc.2022.103230.

[19] J. Wang, X. Zhou, and B. Yi. 2022. Buckling Distortion Investigation During Thin Plates Butt Welding with

Considering Clamping Influence. *CIRP J Manuf Sci Technol.* 37: 278-290. Doi: 10.1016/j.cirpj.2022.02.008.
[20] S. E. Chidiac, F. A. MirzaJ, and D. S. Wilkins. 1994. 'A Simplified Welding Arc Model by the Finite Element Method. *Comput Struct*. 53(5): 1235-1241. Doi: https://DOI.org/10.1016/0045-7949(94)90171-6.
[21] T. L. Teng, P. H. Chang, and W. C. Tseng. 2003. Effect of Welding Sequences on Residual Stresses. *Comput Struct.* 81(5): 273-286. Doi: 10.1016/S0045-7949(02)00447-9.
[22] Z. Barsoum and A. Lundbäck. 2009. Simplified FE Welding Simulation of Fillet Welds - 3D Effects on the Formation Residual Stresses. *Eng Fail Anal.* 16(7): 2281-2289. Doi: 10.1016/j.engfailanal.2009.03.018.
[23] D. Klobčar, J. Tušek, and B. Taljat. 2004. Finite Element Modeling of GTA Weld Surfacing Applied to Hot-Work Tooling. *Comput Mater Sci*. 31(3-4): 368-378. Doi: 10.1016/j.commatsci.2004.03.022.
[24] M. A. Wahab, M. J. Painter, and M. H. Davies. 1998. The Prediction of the Temperature Distribution and Weld Pool Geometry in the Gas Metal Arc Welding Process. *J Mater Process Technol.* 77: 233-239. Doi: 10.1016/S0924-0136(97)00422-6
[25] B. Q. Chen, M. Hashemzadeh and C. G. Soares. 2018. Validation of Numerical Simulations with X-ray Diffraction Measurements of Residual Stress in Butt-welded Steel Plates. *Ships and Offshore Structures.* 13(3): 273-282. Doi: 10.1080/17445302.2017.1368122.